Shape competition and shape coexistence in ^{75}Br

G. Z. Solomon, G. D. Johns,* R. A. Kaye,† and S. L. Tabor
Department of Physics, Florida State University, Tallahassee, Florida 32306
(Received 24 August 1998)

High-spin states in ^{75}Br were populated to investigate shape competition and shape coexistence phenomena in the single and three-quasiparticle regions. The thin-target experiment ^{48}Ti(^{30}Si,$p2n$)^{75}Br at 90 MeV was performed using the FSU Tandem-LINAC accelerator facility, and the FSU-PITT array of 10 Compton-suppressed Ge detectors for the collection of γ-γ coincidence data. Construction of level schemes and assignments of decays, excitation energies, spins, and parities were achieved through examination of coincidence data, relative intensity measurements, and angular correlation analysis. A rotational sequence with band-head spin-parity $J^{\pi}=\frac{9}{2}^{+}$ was found and is compared to a similar band in ^{77}Br. A negative-parity three-quasiparticle band exhibiting rigid rotation was also discovered. In total, 65 new transitions and 36 new excitation states were added to the level scheme. Cranked-shell, Hartree-Fock-Bogoliubov, and particle-rotor coupling models are used in the interpretation. [S0556-2813(99)00903-6]

PACS number(s): 23.20.Lv, 21.10.Re, 21.60.Ev, 27.50.+e

I. INTRODUCTION

The complex behavior exhibited by nuclei in the $A\approx 80$ region gives insight into the competition between single particle and collective modes, and there are straightforward examples of these nuclei whose collective rotational structures are influenced by quasiparticle (qp) excitations. When both the proton and neutron numbers in this region lie close to midshell ($Z=N=39$), high deformation [1–3] and rigid rotational behavior are common. As Z or N vary from midshell, transitional effects may be found. These include shape coexistence [4–6], where very different values of γ may be found for the same nucleus, but in bands of different π or K quantum numbers. Shape competition [7,8] with associated γ softness [9], where oblate and prolate shapes in bands of the same π and K lie close in energy, also occurs. At the $N=50$ shell spherical shell-model behavior [10] is observed. Variations in the coupling between quasiparticles and the core can lead to rapid shape changes [11] and varying degrees of signature splitting [11–16]. Because of its high intrinsic spin, the unique-parity $g_{9/2}$ orbital plays a large role in the structure of yrast and near yrast high-spin states in the $A\approx 80$ region.

Within a family of odd-Z isotopes or odd-N isotones, which should have similar single-particle configurations, γ may vary considerably, as has been observed in the $N=41$ isotones [17]. Still, it is not unreasonable to expect that the isotopes of bromine should have gross similarities.

A common feature of the odd-A Br isotopes is the large signature splitting in the $g_{9/2}$ yrast bands, leading to level inversion in most cases. Because of the inversion, the band of unfavored signature $\alpha=-\frac{1}{2}$ ($J^{\pi}=\frac{7}{2}^{+}$, $\frac{11}{2}^{+}$, etc.) is often difficult to locate and identify. It is not known in ^{73}Br [18] although the band of favored signature has been studied up to spin $\frac{45}{2}^{+}$. However, the candidate unfavored signature band in ^{77}Br has been observed [19] to the $\frac{35}{2}^{+}$ state.

Theoretical calculations of the band-head energies and deformations in ^{75}Br [16] also predicted a low-lying $\frac{9}{2}^{+}$ band-head based on a $g_{9/2}$ oblate orbital, but no experimental candidates were observed. However, an extra rotational band based on an excited $\frac{9}{2}^{+}$ state had been previously observed in ^{77}Br [24,14] although no interpretation for this band has been presented.

The present investigation was undertaken to search for and interpret nonyrast bands in ^{75}Br.

Initial investigation of ^{75}Br in β-decay studies [20] established several low-spin states. Subsequent work [21,22] extended the yrast sequence up to a tentative ($\frac{25}{2}^{+}$) level at 3868 keV and demonstrated a large signature splitting leading to level inversions. The negative-parity yrast pair was observed up to a tentative ($\frac{25}{2}^{-}$) level at 4348 keV with much lower signature splitting. Significant additions to the level scheme, including lifetime measurements, were made [16] in the ^{62}Ni(^{16}O,$p2n$) and ^{66}Zn(^{12}O,$p2n$) experiments. Excited states reaching spin $\frac{33}{2}$ were established for both parities, and the deformations of low-lying states were deduced to fall in the range $0.28\lesssim\beta_2\lesssim 0.35$. In the latest [23] investigation employing the ^{58}Ni(^{24}Mg,$\alpha 3p$) reaction, states up to spins of ($\frac{45}{2}^{+}$) and ($\frac{49}{2}^{-}$) were determined.

II. EXPERIMENTAL METHODS

The ^{48}Ti(^{30}Si,$2np$) reaction at 90 MeV was employed to populate states in ^{75}Br. The ^{30}Si beam was obtained from the 3.1% isotopic abundance in a natural Si sample and accelerated by the Florida State University Tandem-LINAC facility. The 190 μg/cm^2 thick target was enriched to 99% in ^{48}Ti. Prompt γ-γ coincidences were detected using the Pitt-FSU combined detector array [25] with ten Compton-suppressed Ge detectors. Two detectors were placed at 35°, four at 145°, and the remainder at 90° relative to the beam line. The front face of each detector was positioned approxi-

*Present address: Los Alamos National Laboratory, Los Alamos, NM 87545.
†Present address: Physics Division, Argonne National Laboratory, Argonne, IL 60439.

mately 18 cm from the target.

The dominant product in this experiment was ^{75}Br, so known lines of energies 119.5, 563.0, 830.1, and 1045.3 keV from this nucleus were used for an internal energy calibration. This internal calibration provided an automatic compensation for Doppler shifting. A total of 250 million γ-γ coincidence events were collected from this experiment. Of these, approximately 34% were associated with ^{75}Br.

III. ANALYSIS

A. The level scheme

The γ-γ coincidence events were histogrammed into a RADWARE [26] matrix with a dispersion of 1.0 keV/channel. This was the primary data set used for construction of the level scheme. A secondary array was constructed for angular correlation analysis. Since the 35° and 145° detectors are symmetric with respect to 90°, the array was constructed with 90° data on one axis and 35° or 145° data on the other. Gates from this array were used to determine multipolarities of the γ-ray transitions by calculating directional correlation of oriented nuclei (DCO) ratios according to

$$R_{\mathrm{DCO}}=\frac{I_\gamma(\text{at } 35°,145°;\ \text{gated by } \gamma_G \text{ at } 90°)}{I_\gamma(\text{at } 90°;\ \text{gated by } \gamma_G \text{ at } 35°,145°)}, \quad (1)$$

where I_γ is the intensity of the γ ray of interest. In all cases, the γ_G chosen had been determined to be a electric quadrupole transition. In this case the DCO ratios for other stretched electric quadrupole ($E2$) transitions so observed are expected to have values close to 1, while $\Delta I=1$ transitions can have values ranging from 0 to 2 depending on the multipole mixing ratio δ. If the $M1/E2$ mixing ratio is small, then the DCO ratio is expected [4] to be near 0.5.

The present level schemes, shown in Figs. 1 and 2, were deduced from coincidence spectra generated by gating techniques. Transition placement in the level scheme and relative intensities were determined from the primary RADWARE matrix. Multipolarities of the transitions were assigned based on the DCO ratios where possible, and on systematics where not. In the latter cases, the spins are shown in parentheses where no previous assignments were found in the literature.

Results of the level determinations for ^{75}Br, with energies, intensities, multipolarities, DCO ratios and spin assignments are shown in Table I. Altogether more than 60 new transitions were identified, leading to 36 new excitation states.

1. The positive-parity bands

The positive-parity yrast band of favored signature ($\alpha=+\frac{1}{2}$) (band A in Fig. 1) was established [22] to a tentative ($\frac{25}{2}^+$) level at 3868 keV and later extended [23] to ($\frac{45}{2}^+$) at 12206 keV. The current investigation confirms the previously observed yrast transitions, except for the reported [23] 2026 keV transition, which has been replaced by a 1956 keV transition. These transitions have DCO ratios consistent with stretched electric quadrupole transitions, and so firm spin and parity assignments have been made up to the $\frac{41}{2}^+$ state.

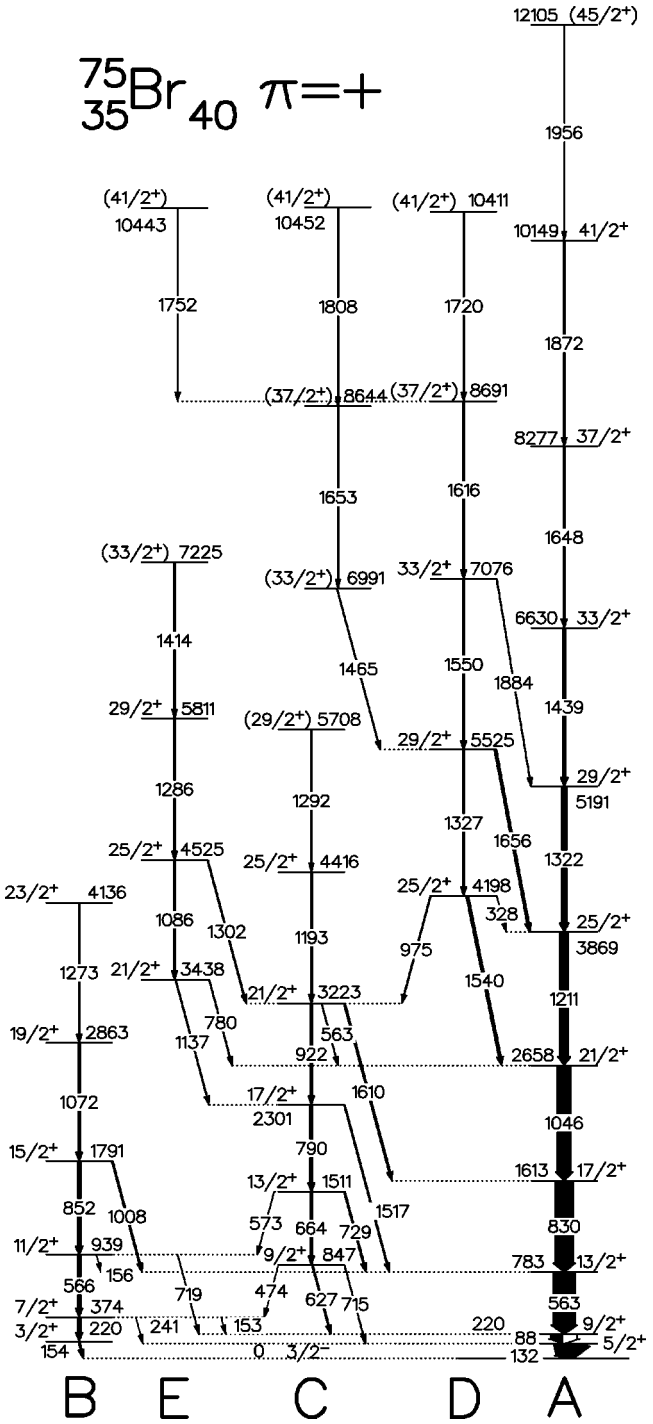

FIG. 1. The positive-parity level scheme of ^{75}Br deduced from the present work.

Four states up to a spin of ($\frac{19}{2}^+$) in the unfavored band (B) were previously identified in ^{75}Br [23], and these transitions have been confirmed with an additional 1273 keV decay added. Firm spin and parity assignments have been made in this band to the $\frac{23}{2}^+$ state.

Prior to the current work, there were no known analogues in the neighboring Br isotopes for the excited $\frac{9}{2}^+$ band in ^{77}Br. An additional positive-parity band (C) has been established in the present work, based on a new excited $\frac{9}{2}^+$ state at 847 keV. This band extends to ($\frac{29}{2}^+$). The DCO ratios of all but the last transition within this band are consistent with

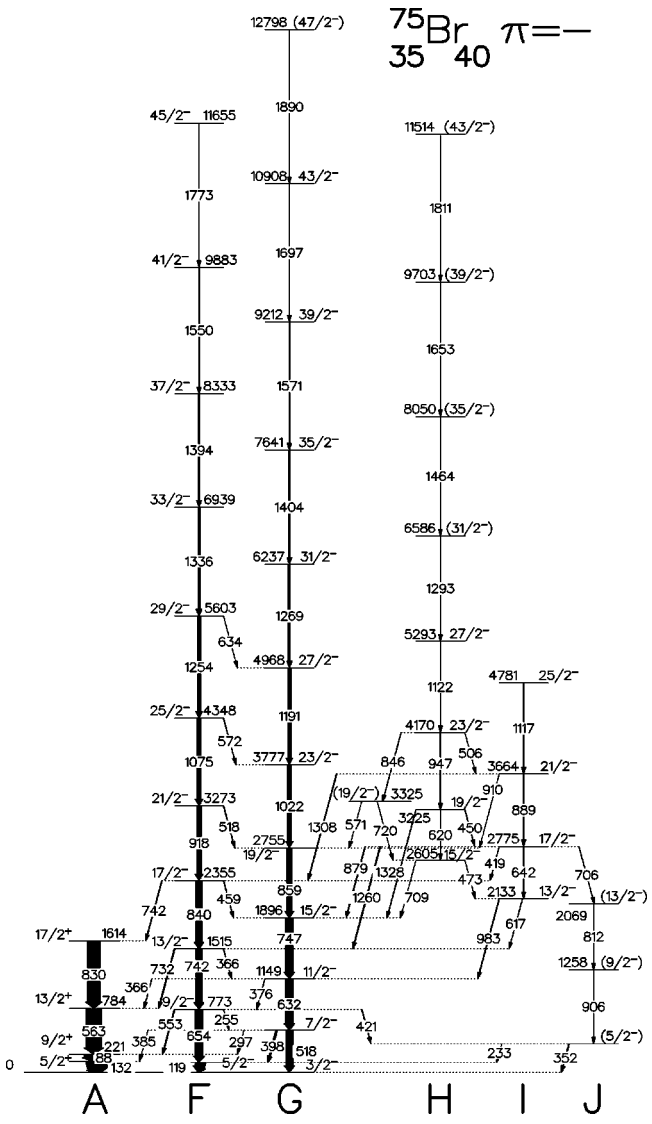

FIG. 2. The negative-parity level scheme of ^{75}Br deduced from the present work.

stretched $E2$ decay, while no DCO ratio could be measured for this last decay. This band is analogous to the extra $\frac{9}{2}^+$ band in ^{77}Br as it ''bleeds out'' to all available positive-parity states, appears to have no observable signature partner, and was not extended to high spin.

Figure 3 shows the summed spectrum of gates on the 664, 790, and 992 keV transitions in this band. The 563 and 88 keV transitions at the bottom of the yrast sequence show clearly in this spectrum, as does the 132 keV $\frac{5}{2}^+ \rightarrow \frac{3}{2}^-$ decay. Many of the new positive-parity transitions may be observed in this spectrum. Figure 4 is shown here to make firm the assignment of this new band to ^{75}Br. This gate on the 132 keV $\frac{5}{2}^+ \rightarrow \frac{3}{2}^-$ transition shows most strongly the positive-parity yrast sequence. It also shows the transitions in the new $\frac{9}{2}^+$ band, as well as the connecting transitions.

Several additional excited positive-parity bands were also observed. The two strongest are labeled D and E in Fig. 1, and two shorter higher-lying decay sequences are positioned somewhat above bands C and E to save space in the level scheme.

2. The negative-parity bands

Early experiments had established [21,22] the negative-parity yrast band pair (F and G) up to a tentative ($\frac{25}{2}^-$) level at 4348 keV. In the latest investigation [23], the negative-parity structure was extended to spin states of ($\frac{49}{2}^-$). These states were confirmed in the present work, with firm spin and parity assignments made up to the $\frac{45}{2}^-$ level.

An additional negative parity structure (band H) was found in the present work. A sequence of 6 transitions, 947, 1122, 1293, 1464, 1653, and 1811 keV are in strong coincidence with each other and the low-spin negative parity states of ^{75}Br. These states bleed out to the negative-parity low-spin states, but not along any preferred path. The 620 keV decay at the bottom of this sequence may either be a low-spin continuation of the sequence, or the strongest ''bleed-out.'' Spectra of the 1122 and 620 keV transitions are compared in Figs. 5 and 6. It should be noted that these gates are very narrow (1 keV wide), to reduce contamination from strong decays in competing residual channels. All the transitions connecting the new band with the known structures are visible in the 1122 keV gate, but it is clear that their intensity, relative to the in-band decays, is not large. The second short sequence of γ rays (band I) including a 1117, 889, and, perhaps, a 642 keV transition, may be the signature partner to this band. A series of three γ rays of energy 706, 812 and 906 keV (J) connect these bands to the previously [21] observed state at 352 keV. Reported decays out of this state of 233 and 352 keV have been confirmed, and an additional 421 keV decay out of the $\frac{9}{2}^-$ level at 773 keV to this state has been added.

IV. DISCUSSION

A. Positive-parity bands

Several new structures have been observed in ^{75}Br in the current work. Interpretation of these structures is aided by the use of cranked-shell-model analysis techniques, which can illuminate details of band crossings, signature splitting and the behavior of the moments of inertia.

In Fig. 7, the kinematic moment of inertia ($J^{(1)}=I_x/\omega$) of the yrast positive-parity band in ^{75}Br is compared with those for the extra bands with band-head spin-parity $\frac{9}{2}^+$ and energies 847 keV (^{75}Br) and 783 keV (^{77}Br [19]). In each of the three cases the moments approach the rigid body value and remain approximately at that value until a frequency of about $\hbar\omega=0.6$ MeV where the extra $\frac{9}{2}^+$ bands (band C and ^{77}Br) end, and the positive-parity yrast band (band A) increases in curvature, indicative of quasiparticle alignment and a structure change to $3qp$. For the yrast band in ^{75}Br, this crossing, which occurs at $\hbar\omega\approx 0.65$ MeV has been interpreted [16] as a $\nu g_{9/2}$ alignment, since the lowest $\pi g_{9/2}$ crossing is Pauli blocked. No alignment is evident for the extra bands.

All the newly discovered positive-parity states in ^{75}Br appear to have signature $\alpha=+\frac{1}{2}$. For the extra $\frac{9}{2}^+$ bands (band C and the corresponding band in ^{77}Br), the behavior of the moments of inertia, converging to about $21\hbar^2$/MeV, is in agreement with previously observed trends [27]. However, these extra $\frac{9}{2}^+$ bands saturate to a higher value, closer to the rigid-body value, than exhibited by the ground state $g_{9/2}$ band within the region where all three are observed. If these

TABLE I. Energies, intensities, and DCO ratios of γ decays in ^{75}Br.

E_x (keV)	I_i^π	I_f^π	E_γ (keV)	Intensity	R_{DCO}
131.9	$\frac{5}{2}^+$	$\frac{3}{2}^-$	131.9(5)	144 [a]	
219.8	$\frac{9}{2}^+$	$\frac{5}{2}^+$	87.9(5)	53	
782.6	$\frac{13}{2}^+$	$\frac{9}{2}^+$	562.7(1)	100	0.97(18) [b]
1612.5	$\frac{17}{2}^+$	$\frac{13}{2}^+$	829.9(1)	81	1.06(13)
2658.0	$\frac{21}{2}^+$	$\frac{17}{2}^+$	1045.5(1)	60	1.00(01)
3869.1	$\frac{25}{2}^+$	$\frac{21}{2}^+$	1211.1(1)	38	1.03(07)
5191.0	$\frac{29}{2}^+$	$\frac{25}{2}^+$	1321.9(1)	22	0.96(06)
6629.5	$\frac{33}{2}^+$	$\frac{29}{2}^+$	1438.5(2)	13	0.99(03)
8277.3	$\frac{37}{2}^+$	$\frac{33}{2}^+$	1647.8(2)	6	0.85(16)
10149.0	$\frac{41}{2}^+$	$\frac{37}{2}^+$	1872.3(4)	4	1.01(12)
12105	$(\frac{45}{2}^+)$	$\frac{41}{2}^+$	1956(1)	<1	
154.4	$\frac{3}{2}^+$	$\frac{3}{2}^-$	154.4(1)	7	0.63(1) [b]
373.6	$\frac{7}{2}^+$	$\frac{3}{2}^+$	219.5(2)	12 [a]	
		$\frac{9}{2}^+$	153(1)	<1	0.63(1) [b]
		$\frac{5}{2}^+$	241.4(9)	<1	
939.0	$\frac{11}{2}^+$	$\frac{7}{2}^+$	565.5(1)	13	0.96(5)
		$\frac{9}{2}^+$	719.2(9)	1	0.39(18)
		$\frac{13}{2}^+$	156.2(9)	1	0.50(7)
1790.5	$\frac{15}{2}^+$	$\frac{11}{2}^+$	851.5(1)	14	0.97(6)
		$\frac{13}{2}^+$	1007.6(9)	6	1.23(8)
2862.9	$\frac{19}{2}^+$	$\frac{15}{2}^+$	1072.4(2)	11	0.94(7)
4136.3	$\frac{23}{2}^+$	$\frac{19}{2}^+$	1273.4(9)	5	1.35(16)
847.0	$\frac{9}{2}^+$	$\frac{9}{2}^+$	627.0(9)	5	0.92(7)
		$\frac{5}{2}^+$	715.2(9)	2	0.98(7)
		$\frac{7}{2}^+$	473.6(9)	<1	
1511.4	$\frac{13}{2}^+$	$\frac{9}{2}^+$	664.1(9)	7	1.04(10)
		$\frac{13}{2}^+$	728.8(9)	6	0.88(4)
		$\frac{11}{2}^+$	572.9(9)	1	0.48(6)
2301.2	$\frac{17}{2}^+$	$\frac{13}{2}^+$	789.8(9)	11	1.07(5)
		$\frac{13}{2}^+$	1516.9(9)	5	0.85(4)
3222.7	$\frac{21}{2}^+$	$\frac{17}{2}^+$	921.7(9)	8	0.94(9)
		$\frac{21}{2}^+$	562.8(9)	2	
		$\frac{17}{2}^+$	1609.9(9)	7	0.76(2)
4416.1	$\frac{25}{2}^+$	$\frac{21}{2}^+$	1193.4(9)	5	1.14(18)
5708.3	$(\frac{29}{2}^+)$	$\frac{25}{2}^+$	1292.2(9)	1	
3438.2	$\frac{21}{2}^+$	$\frac{17}{2}^+$	1137.0(9)	3	1.11(12)
		$\frac{21}{2}^+$	780(2)	3	0.90(8)
4524.5	$\frac{25}{2}^+$	$\frac{21}{2}^+$	1086.3(9)	5	1.26(17)
		$\frac{21}{2}^+$	1302.0(9)	4	
5810.6	$\frac{29}{2}^+$	$\frac{25}{2}^+$	1286.1(9)	6	1.28(13)
7225	$(\frac{33}{2}^+)$	$\frac{29}{2}^+$	1414(1)	3	
6990.8	$(\frac{33}{2}^+)$	$\frac{29}{2}^+$	1465.4(9)	3	0.89(15)
8643.9	$(\frac{37}{2}^+)$	$(\frac{33}{2}^+)$	1653.1(9)	2	
10451.7	$(\frac{41}{2}^+)$	$(\frac{37}{2}^+)$	1807.8(9)	2	
4197.8	$\frac{25}{2}^+$	$\frac{21}{2}^+$	975.1(9)	4	1.18(13)
		$\frac{21}{2}^+$	1539.8(9)	11	0.95(28)
		$\frac{25}{2}^+$	328(1)	<1	0.50(21)
5525.4	$\frac{29}{2}^+$	$\frac{25}{2}^+$	1327.4(9)	5	
		$\frac{25}{2}^+$	1656.4(9)	10	1.00(10)
7075.5	$\frac{33}{2}^+$	$\frac{29}{2}^+$	1550.3(9)	7	0.98(9)
		$\frac{29}{2}^+$	1884.2(9)	2	
8691.3	$(\frac{37}{2}^+)$	$\frac{33}{2}^+$	1615.8(9)	6	

TABLE I. (*Continued*).

E_x (keV)	I_i^π	I_f^π	E_γ (keV)	Intensity	R_{DCO}
10443	$(\frac{41}{2}^+)$	$(\frac{37}{2}^+)$	1752(1)	3	
10411	$(\frac{41}{2}^+)$	$(\frac{37}{2}^+)$	1720(1)	3	
517.8	$\frac{7}{2}^-$	$\frac{3}{2}^-$	517.8(1)	52	0.75(5)
		$\frac{5}{2}^-$	398.2(1)	10	0.50(7)
		$\frac{9}{2}^+$	297.0(9)	<1	0.62(13)
		$\frac{5}{2}^+$	385.1(9)	<1	0.63(7)
1149.4	$\frac{11}{2}^-$	$\frac{7}{2}^-$	631.6(1)	46	0.84(6)
		$\frac{9}{2}^-$	376.0(1)	1	0.47(12)
		$\frac{13}{2}^+$	365.9(1)	1	0.51(25)
1896.1	$\frac{15}{2}^-$	$\frac{11}{2}^-$	746.7(1)	46	0.97(9)
2755.0	$\frac{19}{2}^-$	$\frac{19}{2}^-$	858.9(1)	34	1.04(12)
3776.9	$\frac{23}{2}^-$	$\frac{19}{2}^-$	1021.9(1)	24	1.00(6)
4967.9	$\frac{27}{2}^-$	$\frac{23}{2}^-$	1191.0(1)	19	1.03(2)
6236.9	$\frac{31}{2}^-$	$\frac{27}{2}^-$	1269.0(1)	13	1.05(7)
7640.9	$\frac{35}{2}^-$	$\frac{31}{2}^-$	1404.0(1)	8	1.03(11)
9211.4	$\frac{39}{2}^-$	$\frac{35}{2}^-$	1570.7(2)	5	1.10(14)
10908.1	$\frac{43}{2}^-$	$\frac{39}{2}^-$	1696.7(4)	2	1.00(14)
12797.8	$(\frac{47}{2}^-)$	$\frac{43}{2}^-$	1889.7(6)	1	
119.3	$\frac{5}{2}^-$	$\frac{3}{2}^-$	119.3(1)	57	0.67(3)
773.2	$\frac{9}{2}^-$	$\frac{5}{2}^-$	653.9(1)	48	0.87(4)
		$\frac{7}{2}^-$	255.2(1)	1	0.43(9)
		$\frac{9}{2}^+$	552.6(2)	4	0.88(6)
		$(\frac{5}{2}^-)$	420.6(9)	2	
1515.4	$\frac{13}{2}^-$	$\frac{9}{2}^-$	742.3(1)	40	1.00(9)
		$\frac{11}{2}^-$	365.9(1)	1	0.54(5)
		$\frac{13}{2}^+$	732.0(9)	5	0.88(1)
2355.1	$\frac{17}{2}^-$	$\frac{13}{2}^-$	839.7(1)	40	1.00(12)
		$\frac{15}{2}^-$	458.5(1)	2	0.40(4)
		$\frac{17}{2}^+$	742.0(1)	3	
3273.0	$\frac{21}{2}^-$	$\frac{17}{2}^-$	917.9(1)	30	1.03(2)
		$\frac{19}{2}^-$	517.8(1)	2	
4348.3	$\frac{25}{2}^-$	$\frac{21}{2}^-$	1075.2(1)	27	1.02(5)
		$\frac{23}{2}^-$	572.2(1)	1	0.49(19)
5602.5	$\frac{29}{2}^-$	$\frac{25}{2}^-$	1254.2(1)	20	1.06(13)
		$\frac{27}{2}^-$	634.0(9)	<1	0.82(7)
6938.8	$\frac{33}{2}^-$	$\frac{29}{2}^-$	1336.3(1)	16	1.01(5)
8333.0	$\frac{37}{2}^-$	$\frac{33}{2}^-$	1394.2(1)	10	1.03(2)
9882.5	$\frac{41}{2}^-$	$\frac{37}{2}^-$	1549.5(2)	6	1.05(3)
11655.0	$\frac{45}{2}^-$	$\frac{41}{2}^-$	1772.5(3)	3	0.97(13)
2132.8	$\frac{13}{2}^-$	$\frac{11}{2}^-$	983.3(9)	3	0.84(4)
		$\frac{13}{2}^-$	617(1)	1	
2775.1	$\frac{17}{2}^-$	$\frac{13}{2}^-$	642.3(9)	3	0.91(6)
		$\frac{15}{2}^-$	879.1(9)	3	0.95(21)
		$\frac{13}{2}^-$	1259.7(9)	4	
		$\frac{17}{2}^-$	419.5(9)	1	
		$(\frac{13}{2}^-)$	706.1(1)	1	
3664.2	$\frac{21}{2}^-$	$\frac{17}{2}^-$	889.3(9)	7	1.07(27)
		$\frac{19}{2}^-$	909.7(9)	1	
		$\frac{17}{2}^-$	1308.4(9)	3	0.97(11)
4781.0	$\frac{25}{2}^-$	$\frac{21}{2}^-$	1116.8(9)	7	1.10(37)
2605.3	$\frac{15}{2}^-$	$\frac{13}{2}^-$	472.9(9)	1	
		$\frac{15}{2}^-$	709.4(9)	<1	0.98(10)

TABLE I. (*Continued*).

E_x (keV)	I_i^π	I_f^π	E_γ (keV)	Intensity	R_{DCO}
3224.9	$\frac{19}{2}^-$	$\frac{15}{2}^-$	619.9(9)	2	0.94(8)
		$\frac{17}{2}^-$	450.0(9)	2	0.62(6)
		$\frac{15}{2}^-$	1328.4(9)	2	0.95(10)
4170.4	$\frac{23}{2}^-$	$\frac{19}{2}^-$	946.5(9)	4	0.99(7)
		$\frac{21}{2}^-$	505.8(9)	<1	
		$\frac{19}{2}^-$	846(2)	1	0.76(30)
5292.5	$\frac{27}{2}^-$	$\frac{23}{2}^-$	1122.1(9)	3	1.10(37)
6585.9	$(\frac{31}{2}^-)$	$\frac{27}{2}^-$	1293.4(9)	3	
8050.3	$(\frac{35}{2}^-)$	$(\frac{31}{2}^-)$	1464.4(9)	1	
9703	$(\frac{39}{2}^-)$	$(\frac{35}{2}^-)$	1653(1)	1	
11514	$(\frac{43}{2}^-)$	$(\frac{39}{2}^-)$	1811(1)	1	
3325.1	$(\frac{19}{2}^-)$	$\frac{15}{2}^-$	719.9(9)	1	
		$\frac{19}{2}^-$	571(2)	1	
352.1	$(\frac{5}{2}^-)$	$(\frac{3}{2}^-)$	352.1(9)	3	
		$\frac{5}{2}^-$	232.7(9)	<1	
1257.8	$(\frac{9}{2}^-)$	$(\frac{5}{2}^-)$	905.7(9)	1	
2069.2	$(\frac{13}{2}^-)$	$(\frac{9}{2}^-)$	811.6(9)	1	

[a]Lower limit.
[b]Combined DCO ratio of doublet.

extra bands are built on a quasiproton occupation of a high-K oblate orbital arising from the $g_{9/2}$ spherical shell (discussed below), then this quasiproton could well be almost fully aligned, explaining the rapid $J^{(1)}$ saturation. These bands also appear solely $1qp$, as no transitions are observed above the region of the band crossing.

One possible interpretation of band D is that it may represent the continuation of the excited $g_{9/2}$ band in ^{75}Br (band

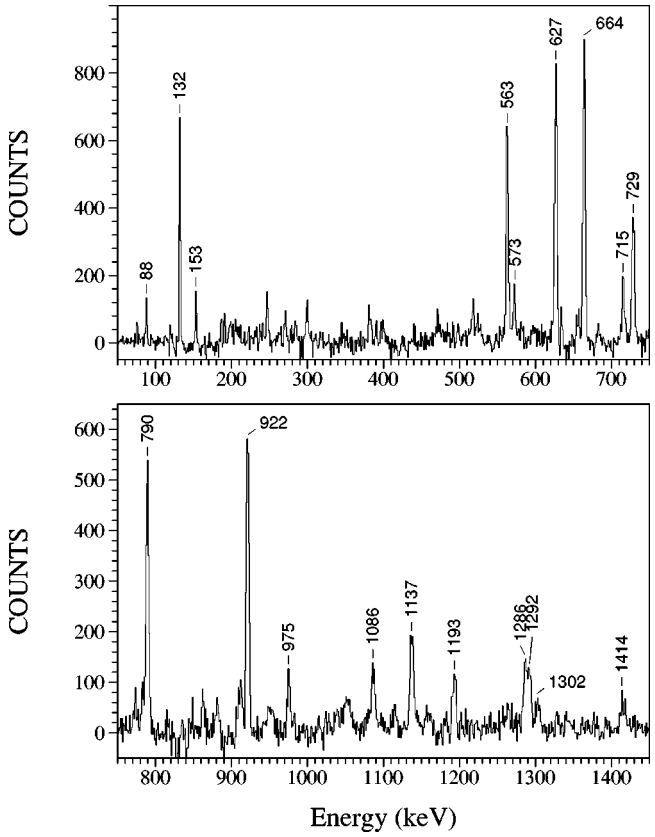

FIG. 3. The spectrum of γ-rays in coincidence with the 664, 790, and 922 keV transitions in the new $\frac{9}{2}^+$ band in ^{75}Br.

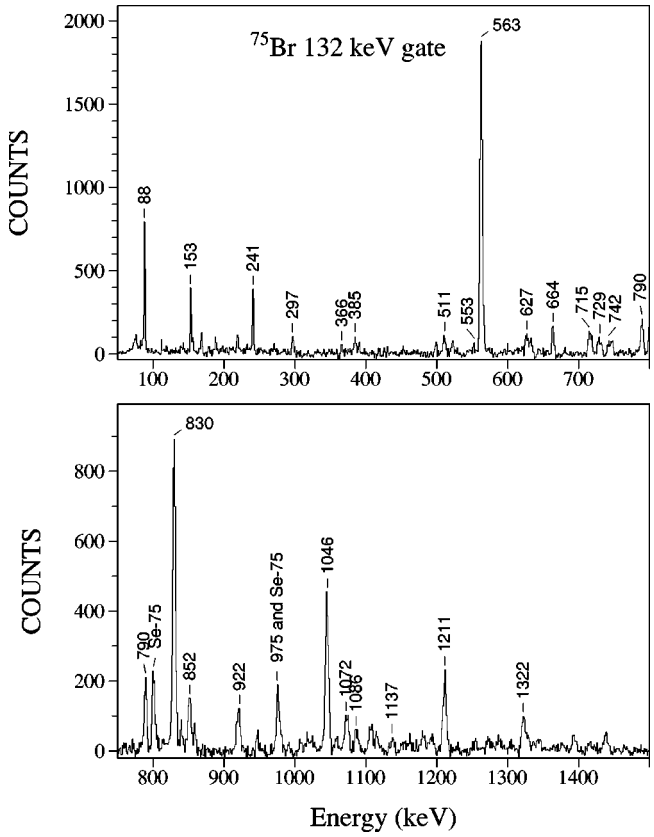

FIG. 4. The spectrum of γ-rays in coincidence with the 132 keV $\frac{5}{2}^+ \rightarrow \frac{3}{2}^-$ transition.

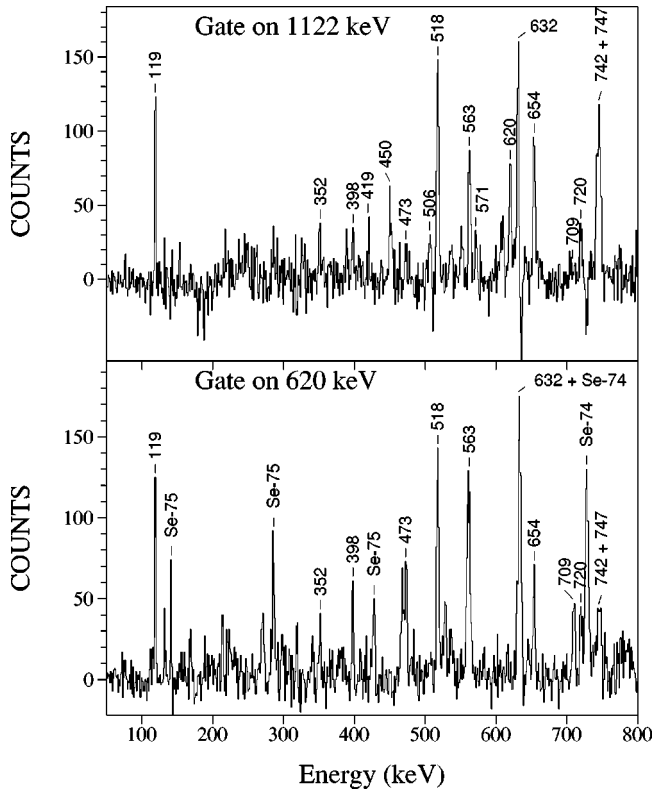

FIG. 5. Spectra of γ-rays in coincidence with the 1122 keV (upper panel) and 620 keV (lower panel) transitions in the range 50 to 800 keV.

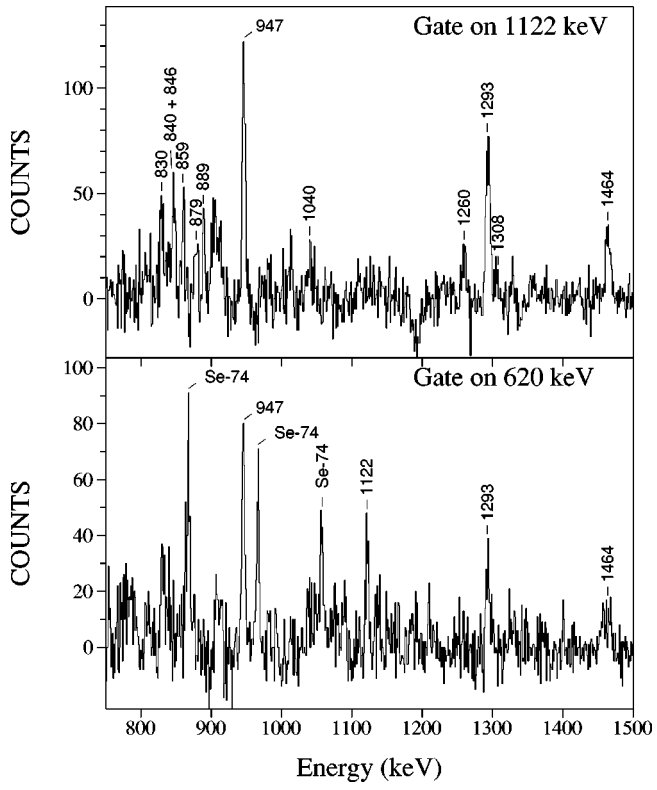

FIG. 6. Spectra of γ-rays in coincidence with the 1122 keV (upper panel) and 620 keV (lower panel) transitions in the range 750 to 1500 keV.

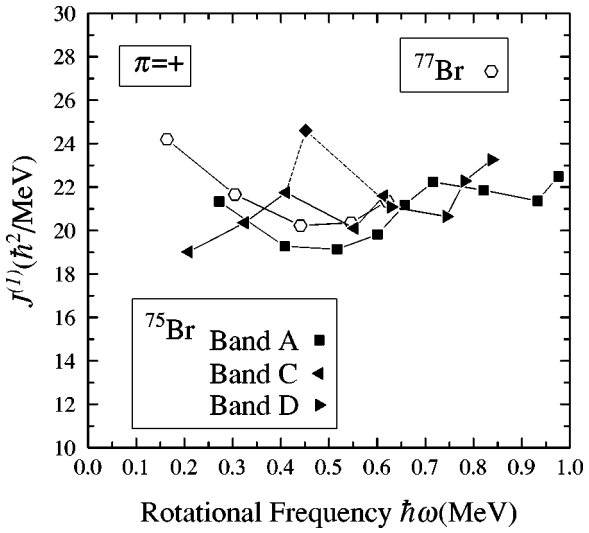

FIG. 7. Kinematic $J^{(1)}$ moments of inertia as a function of rotational frequency ω for the positive-parity yrast band of ^{75}Br and the extra $\frac{9}{2}^+$ bands in ^{75,77}Br with band-head energies 847 and 783 keV, respectively. The filled diamond and dashed lines represent a possible connection between bands C and D. The $\alpha=+\frac{1}{2}$ signature is shown.

C) into the $3qp$ region, via the 975 keV transition $\frac{25}{2}^+ \rightarrow \frac{21}{2}^+$. The kinematic moments of inertia for the possible combined structure are also shown in Fig. 7 with a dashed line and diamond. After the suggested alignment at a frequency of approximately $\hbar\omega=0.45$ MeV the moment returns to the rigid-body value. A second alignment may be evident from the increasing curvature starting at $\hbar\omega=0.75$ MeV. No analogue to band D has been found in ^{77}Br.

Another possible interpretation of band D is that it represents the $1qp$ continuation of the lower $1qp$ portion of band A. In this case, band E might be the $3qp$ aligned structure built on band C. Any of these possible interpretations of bands D and E would imply that $1qp$ and $3qp$ structures are observable over a significant overlapping region.

The Woods-Saxon cranking model of Nazarewicz *et al.* [28] was used to predict the shapes of ^{75}Br. The rotation was treated by means of the cranking approximation with a monopole pairing force. More information about the calculation is given in Refs. [4,29].

Typical total Routhian surfaces (TRS) from the calculations for positive-parity structures in ^{75}Br are shown in Fig. 8. The calculation shown for a rotational frequency of $\hbar\omega \cong 0.3$ MeV is typical of the surface below the first band crossing, while that of 0.7 MeV gives an indication of the shape changes predicted after the alignment. The graphs for the unfavored signature $\alpha=-\frac{1}{2}$ are generally similar to those shown for $\alpha=+\frac{1}{2}$ and are not shown. Some γ sensitivity is predicted for the prolate minimum at low frequency, and there appears to be a second less-favored minimum along the oblate axis. This result was observed in previous [19] results for ^{77}Br, where a more considerable γ softness was predicted in the $1qp$ bands of ^{77}Br, and a weaker oblate structure was also apparent. In both cases, moderately strong deformations of $\beta_2 \approx 0.3$ for ^{77}Br and of $\beta_2 \approx 0.33$ for ^{75}Br

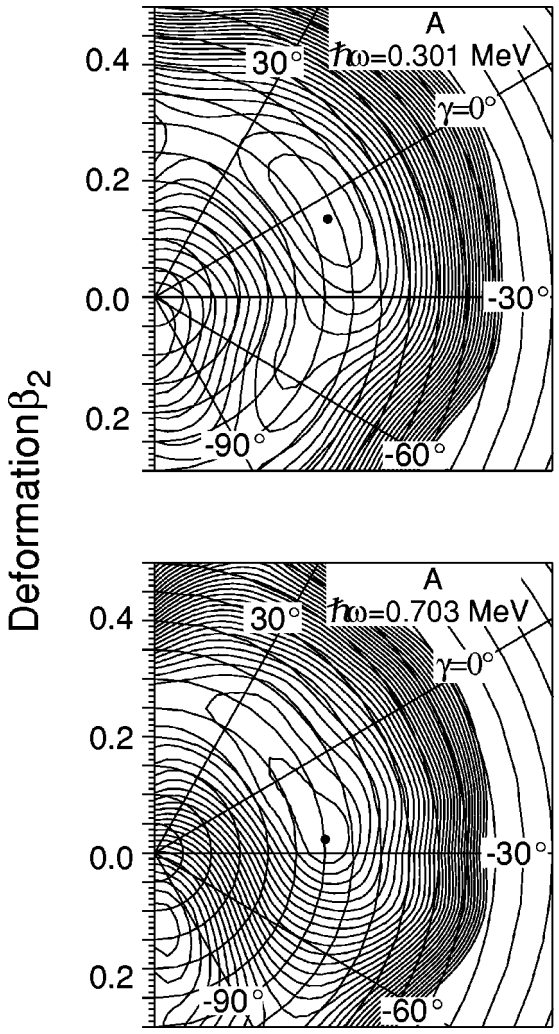

FIG. 8. Theoretical total Routhian surfaces for positive-parity structures in ^{75}Br plotted as a function of the quadrupole deformation parameters β_2 and γ, with the hexadecapole deformation β_4 varied to minimize energy. The top (bottom) plot is for the lowest $\pi=+$, $\alpha=+\frac{1}{2}$ ''A'' configurations, shown at a rotational frequency $\hbar\omega=0.3$ MeV (0.7 MeV).

are predicted, in agreement with the measured [30,16] $B(E2)$ values.

Previous theoretical calculations [16] of the band-head energies and deformations in ^{75}Br predicted the low-lying prolate states of spins $\frac{3}{2}^-$ and $\frac{3}{2}^+$, both of which have been observed experimentally. A $g_{9/2}$ oblate band-head, of spin-parity $\frac{9}{2}^+$, was also predicted, just slightly higher in energy. This band had not been observed previously in ^{75}Br, though a positive-parity band of band-head spin-parity $\frac{9}{2}^+$ has been observed in ^{77}Br [24]. In both nuclei, the TRS plots at $\hbar\omega=0.3$ MeV show a broad minimum extending from the triaxial to oblate axis, with an average quadrupole deformation β_2 of about 0.25. As shape-competition effects are expected to be weaker in the positive-parity than in the negative-parity structures [16], it is possible that these extra $g_{9/2}$ bands found in ^{75,77}Br are the predicted oblate bands.

Calculations of the level energies were made using the triaxial particle-rotor model [31,32] with standard parameters [33] for the modified harmonic oscillator potential. A variable moment of inertia was used for the rotor based on Harris parameters of $J_0=15\hbar^2/\text{MeV}$ and $J_1=3\hbar^4/\text{MeV}^3$, consistent with the cranked-shell model calculations. A Coriolis attenuation factor of $\xi=0.7$ was used in all cases. The nuclear shapes were taken from those predicted by the Hartree-Fock-Bogoliubov cranking calculations of Fig. 8. Calculations were made for oblate and prolate shapes in the positive-parity structures of ^{75}Br and oblate shapes for the positive-parity structures of ^{77}Br. The parameters used appear in Table II.

TABLE II. Rotor-particle-coupling calculation modified oscillator shape parameters for ^{75}Br and ^{77}Br.

Z	A	Parity	Shape	ϵ_2	ϵ_4	γ
35	75	$\pi=+$	prolate	0.29	0.034	4.1°
35	77	$\pi=+$	oblate	−0.2	0.026	26.0°
35	75	$\pi=+$	oblate	−0.5	0.026	23.0°

The results of the particle-rotor model (rotor-particle-coupling, or RPC) calculations are shown for the positive-parity structures in Fig. 9 along with the experimental levels. The RPC results for the yrast positive-parity bands reproduce the large signature splitting and level inversion experimentally observed in ^{75}Br, though the degree of inversion observed is less than predicted. Overall, the agreement is better for ^{75}Br than was the case for previous [19] calculations for ^{77}Br, which did not reproduce the reduction in signature splitting experimentally observed in ^{77}Br above the $\frac{21}{2}^+$ state in that nucleus. This may well be due to a change in triaxiality in ^{77}Br, which was not predicted for the more stable ^{75}Br shape. At higher spins the predicted level energies are somewhat lower than experiment. This phenomenon has often been seen in RPC calculations for bands based on unique-parity orbitals such as the $g_{9/2}$. Such a level depres-

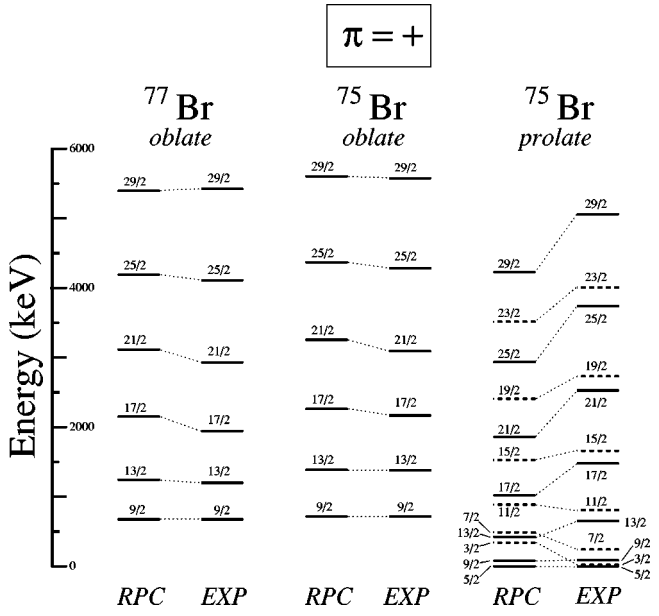

FIG. 9. A comparison of the experimentally deduced positive-parity bands in ^{77}Br and ^{75}Br with particle-rotor model calculations discussed in the text. States with unfavored signature ($\alpha=-\frac{1}{2}$) are drawn with dashed lines to make the comparison of level ordering clearer.

sion was seen in calculations [34] for ^{79}Rb as well as ^{77}Br. Calculations along somewhat similar lines have also been made in the past [24,30]. These calculations also tended to overpredict the degree of signature splitting. For example, the $\frac{7}{2}^+$-$\frac{13}{2}^+$ level ordering is inverted in those calculations as well as the present ones. Those of [30] used a similar deformation of $\beta_2=0.3$, although it is not clear what degree of triaxiality was used.

Since the relative positioning of the oblate and prolate states could not be calculated, the first oblate RPC levels ($\frac{9}{2}^+$) for both ^{75}Br and ^{77}Br were aligned with the experimental ones for the purposes of comparison. That being said, the agreement between theory and experiment under the assumption of an oblate shape due to a $g_{9/2}$ proton in an oblate driving $[404]\frac{9}{2}$ orbital for both nuclei is remarkable.

An excited band of the right signature and spin is predicted in the prolate RPC calculations for both nuclei. However, this band is not a good candidate to represent the extra $\frac{9}{2}$ band found in ^{75,77}Br as, in both cases, it is predicted too high in energy, and, perhaps more telling, the predicted interband decay patterns do not match experiment. This final test of interband feeding patterns could not be applied to the oblate hypothesis.

B. Negative-parity bands

The kinematic moments of inertia for the ground-state negative-parity bands (F and G) of ^{75}Br, which are shown in Fig. 10 (top), increase considerably at low spins and then appear to saturate at the rigid-body value after the first band crossing, to then rise after the second band crossing.

These two alignments can be seen clearly in the $J^{(2)}$ graphs (bottom, Fig. 10) at rotational frequencies of about $\hbar\omega=0.45$ and 0.65 MeV for the $\alpha=+\frac{1}{2}$ signature (band F) and about 0.05 MeV earlier in the $\alpha=-\frac{1}{2}$ signature (band G). The first alignment has been interpreted [16] as a $\pi g_{9/2}$ crossing, which is Pauli-blocked in the positive-parity band. The second has been interpreted as a $\nu g_{9/2}$ crossing, analogous to that seen in the positive-parity band at a similar frequency.

The experimental reduced (single-particle) aligned angular momenta for bands F, G, and H are shown in Fig. 11. The reference rotor which has been subtracted is based on the Harris parameters, $J_0=15\hbar^2/\mathrm{MeV}$ and $J_1=3\hbar^4/\mathrm{MeV}^3$. The ground-state bands F and G see a rise of about 4 units of angular momenta during the first alignment, and about 3 units during the second, consistent with the alignment of a pair of $g_{9/2}$ protons followed by a $g_{9/2}$ neutron alignment.

Signature splitting, as illustrated in a plot of normalized energy differences (Fig. 12) shows an interesting pattern for the ground-state negative-parity bands of several Br isotopes. These energy differences, calculated as $(E_i-E_{i-1})/2I_i$ and plotted as a function of angular momentum, are presented for the negative-parity bands of ^{73,75,77}Br.

At low spins in ^{73,75,77}Br there is very large splitting with the $\alpha=+\frac{1}{2}$ signature favored. Above the first band crossing the $3qp$ region there is an opposing tendency which is strongest in the lightest istopes. It leads to signature inversion with the $\alpha=-\frac{1}{2}$ signature favored in ^{73,75}Br and to reduced splitting with no inversion in ^{77}Br. After the second band crossing, the signature splitting reverts to normal ($\alpha=+\frac{1}{2}$ favored) and increases. This reversion in the $5qp$ region has been observed for the first time in ^{75}Br in the present work. These patterns have been interpreted in ^{75}Br [16] and ^{73}Br [18] as due to changes in the γ deformation parameter. The

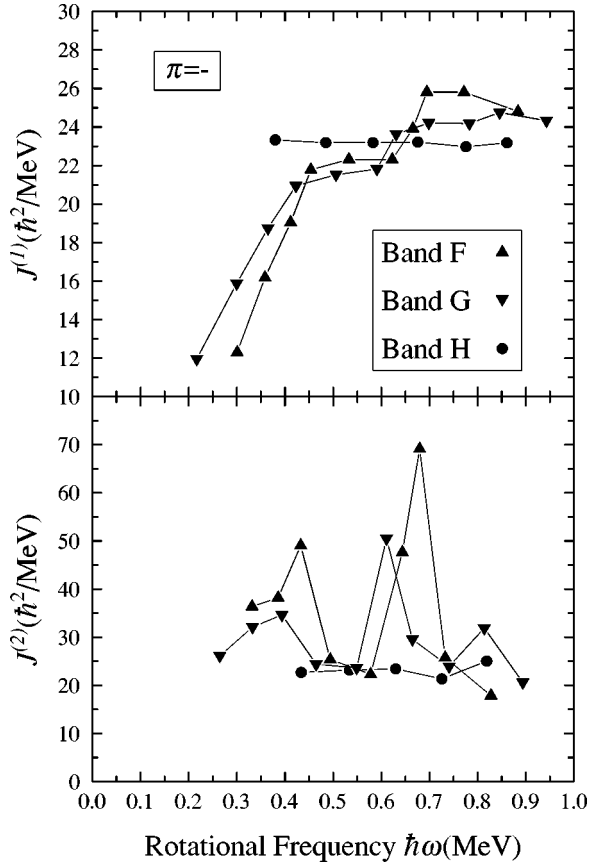

FIG. 10. Kinematic $J^{(1)}$ and dynamic $J^{(2)}$ moments of inertia as a function of rotational frequency ω for the negative-parity bands of ^{75}Br.

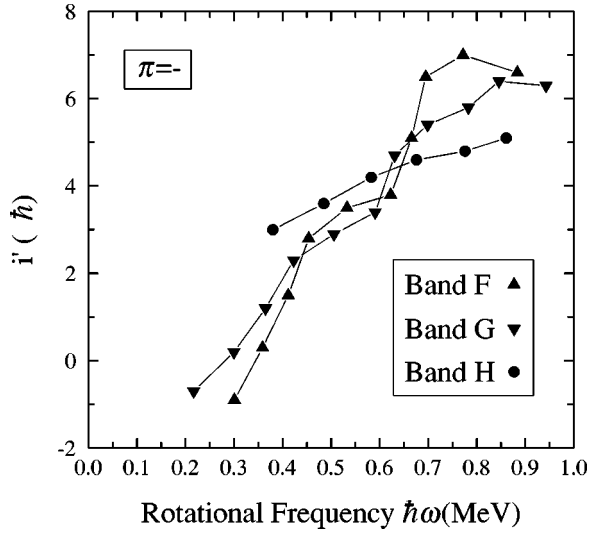

FIG. 11. Graphs of reduced single-particle aligned angular momenta i' versus rotational frequency for the negative-parity bands in ^{75}Br. Harris parameters of $J_0=15\hbar^2/\mathrm{MeV}$ and $J_1=3\hbar^4/\mathrm{MeV}^3$ were used for the reference rotor.

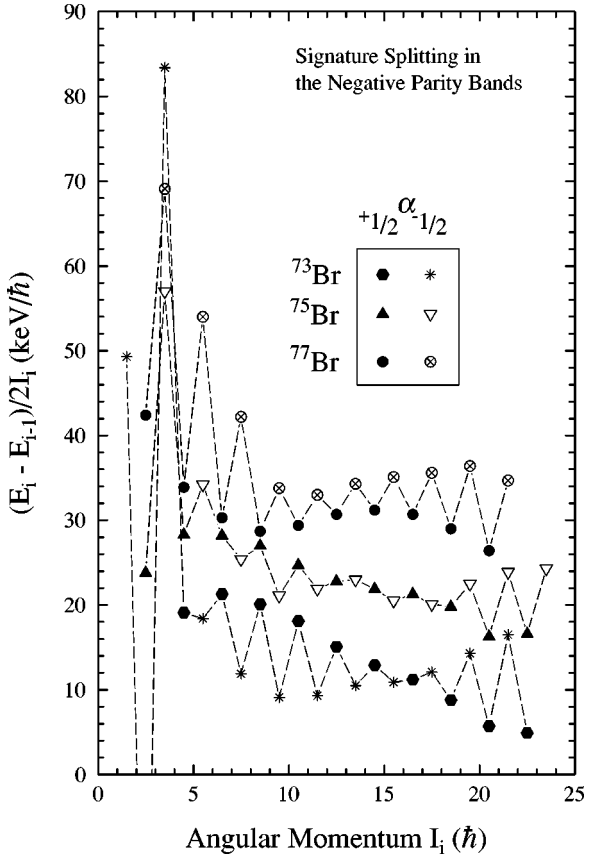

FIG. 12. Normalized energy differences $(E_i - E_{i-1})/2I_i$ in the yrast negative-parity bands in ^{73,75,77}Br. Note that for the purposes of clarity, the ^{77}Br results are offset by $+10$ keV.

first quasiproton alignment drives γ from negative to positive values, while the subsequent quasineutron alignment drives γ back to negative values. The changes in γ appear to be systematic among the odd Br isotopes with the largest changes for the lightest. A rather similar pattern has been observed in the $N=43$ isotones [35]. Together they suggest that signature splitting can be a sensitive indicator of changes in γ in odd-A f-p-g shell nuclei.

TRS calculations for negative-parity structures in ^{75}Br are shown in Fig. 13. Again, considerable γ softness is predicted in the $1qp$ bands ($\hbar\omega \approx 0.3$ MeV), with clear minima along both collective axes. It is reasonable to expect shape-competition effects in the negative-parity bands, as Nilsson prolate orbitals arising from the fp spherical states have oblate structural analogues. No such analogues exist for the low-$Kg_{9/2}$ prolate states [16].

The TRS plots for the negative-parity structures of ^{75}Br after alignment, at $\hbar\omega = 0.7$ MeV, predict little change in the preferred collective shape, and show a similar degree of γ softness as was seen at lower frequencies, unlike the results [19] for ^{77}Br, where the predicted γ softness is greatly reduced, and whose shape was then predicted to become triaxial, with $\gamma \approx -30°$. These differences may correlate to the differences in the behavior of the signature splitting as N approaches shell-closure (see Fig. 12).

An excited negative-parity sequence (band H), with a band-head of spin-parity $\frac{15}{2}^-$ at 2605 keV, was found in the current investigation. This sequence exibited several remarkable characteristics. With excitation energies typically between 400 and 600 keV above the yrast states, this sequence is very rigid, showing little deviation in the values of the moments of inertia. The kinematic moment for band H is shown in Fig. 10 (top) and over the observed frequency range of $\hbar\omega = 0.48$ to 0.98 MeV is very constant, at about the rigid body value. The plot of the dynamic moment of inertia (Fig. 10, bottom) is also very regular, and only at the highest measured frequency does there appear to be any evidence of the beginning of an alignment.

This band is observed primarily in the region where the ground-state negative-parity bands are in $3qp$ or $5qp$ configurations, but itself shows little evidence of a band crossing, and is not observed in the $1qp$ region. For that reason, it is apparent that this sequence is inherently $3qp$ in nature, and any additional angular momentum added to the system

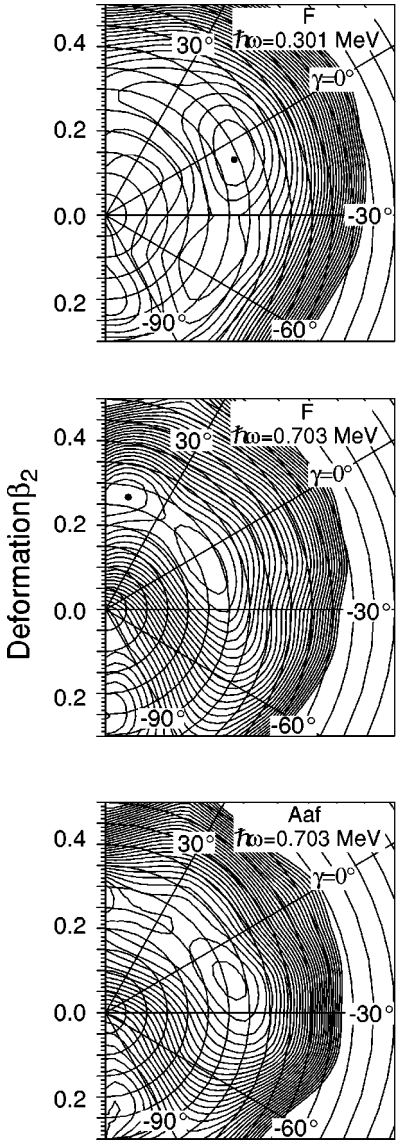

FIG. 13. Theoretical total Routhian surfaces for negative-parity structures in ^{75}Br plotted as a function of the quadrupole deformation parameters β_2 and γ, with the hexadecapole deformation β_4 varied to minimize energy. The top (center) plot is for the lowest $\pi = -$, $\alpha = +\frac{1}{2}$ ''F'' configurations, shown at a rotational frequency $\hbar\omega = 0.3$ MeV (0.7 MeV). The bottom panel shows the calculations for the excited ''Aaf'' configuration.

through single-particle alignment is both gradual and slight, behaving very much like a classic rigid rotor. The curve representing the reduced single-particle aligned angular momenta (Fig. 11) for band H consistently lies between the $3qp$ and $5qp$ sections of the ground-state bands, with only a very gradual addition of perhaps 2 units over the entire measured frequency range. This is interpreted as further support for the identification of band H as a rigid $3qp$ structure.

Additionally, the energies of in-band decays imply that this band is not expected to have deformations much different from that of the ground-state band. Several theoretical three-particle configurations of negative parity and signature $\alpha=-\frac{1}{2}$ were considered, in hopes of finding a configuration predicting characteristics similar to those found experimentally.

Yrast and near yrast configurations of one proton and two neutrons, with the proton in the negative-parity (fp) orbital, have already been accounted for in the $3qp$ region of the ground-state bands. The weak decays from the $\frac{21}{2}^-$, $\frac{19}{2}^-$, and $\frac{17}{2}^-$ states in bands H and I to the ground-state bands have transition strength $B(E2)$ ratios ($B(E2)$ interband/$B(E2)$ intraband) of 6%, 2%, and 6%, respectively. This suggests a configuration differing significantly from that of the ground-state bands. One possiblility is a configuration of the form $\pi g_{9/2}\otimes \nu g_{9/2}\otimes \nu(p\oplus f)$. The TRS calculations provide some confirmation of this suggestion, because, of the $3qp$ negative-parity configurations, only the Aaf configuration, shown in the bottom panel of Fig. 13, was found to have a rather constant shape over the observed frequency range, no sharp alignments, and an energy from 300 to 600 keV above that of the F configuration. This configuration would be doubly-blocked, explaining the lack of further qp alignments.

V. SUMMARY

The high-spin structure of ^{75}Br was investigated using the ^{48}Ti(^{30}Si,$p2n$) reaction at 90 MeV, with the Pitt-FSU γ-detection array and the FSU Tandem-LINAC accelerator facility. Results for ^{75}Br confirmed the level scheme of Ref. [23]. Additionally 65 new transitions were identified, and 36 new excitation states were added. Firm spin and parity assignments were established up to $\frac{41}{2}^+$ and $\frac{45}{2}^-$. Several interesting new band structures were observed.

A new positive-parity band built on an 847 keV $\frac{9}{2}^+$ state appears to represent an oblate $g_{9/2}$ structure co-existing with the prolate $g_{9/2}$ yrast band. The Woods-Saxon cranking calculations predict an excited oblate shape, and the observed band energies agree rather well with oblate RPC calculations. A previously observed $\frac{9}{2}^+$ excited band in ^{77}Br suggests that this shape coexistence extends to other Br isotopes. A new higher-lying positive-parity band of likely $3qp$ structure was also observed, but it is not clear whether it represents an extension of the oblate band.

Analysis of the high-spin region of the negative-parity ground-state band has revealed a return to ''normal'' signature splitting at the $\frac{39}{2}^-$ state, above a region of inverted and reduced splitting. These changes in signature splitting are generally consistent with theoretically predicted changes in the γ shape parameters as first proton, then neutron pairs align.

A newly observed excited, negative-parity band structure exhibits a remarkably constant moment of inertia with no evidence of qp alignments. A suggested $\pi g_{9/2}\otimes \nu g_{9/2}\otimes \nu(p\oplus f)$ configuration appears to account for many of its properties.

ACKNOWLEDGMENTS

We wish to thank W. Nazarewicz for providing the Woods-Saxon cranking model results, and D.C. Radford for software support. This work was supported in part by the U.S. National Science Foundation.

[1] S. L. Tabor, P. D. Cottle, J. W. Holcomb, T. D. Johnson, P. C. Womble, S. G. Buccino, and F. E. Durham, Phys. Rev. C **41**, 2658 (1990).

[2] J. Heese, D. J. Blumenthal, A. A. Chisti, P. Chowdhurry, B. Crowell, P. S. Ennis, C. J. Lister, and Ch. Winter, Phys. Rev. C **43**, R921 (1991).

[3] D. F. Winchell, M. S. Kaplan, J. X. Saladin, H. Takai, J. J. Kolata, and J. Dudek, Phys. Rev. C **40**, 2672 (1989).

[4] E. F. Moore, P. D. Cottle, C. J. Gross, D. M. Headly, U. J. Hüttmeier, S. L. Tabor, and W. Nazarewicz, Phys. Rev. C **38**, 696 (1988).

[5] H. Sun, J. Döring, G. D. Johns, R. A. Kaye, G. Z. Solomon, S. L. Tabor, M. Devlin, D. R. LaFosse, F. Lerma, D. G. Sarantites, C. Baktash, D. Rudolph, C.-H. Yu, I. Y. Lee, A. O. Macchiavelli, I. Birriel, J. X. Saladin, D. F. Winchell, and V. Q. Wood, Phys. Rev. C **59**, 655 (1999).

[6] B. J. Varley, M. Campbell, A. A. Chishti, W. Gelletly, L. Goettig, C. J. Lister, A. N. James, and O. Skeppstedt, Phys. Lett. B **194**, 463 (1987).

[7] R. B. Peircey, J. H. Hamilton, R. Soundranoyagam, A. V. Ramayya, C. F. Maguire, X.-J. Sun, Z. Z. Zhao, R. L. Robinson, J. H. Kim, S. Frauendorf, J. Döring, L. Funke, G. Winter, J. Roth, L. Cleemann, J. Eberth, W. Neumann, J. C. Wells, J. Lin, A. C. Rester, and H. K. Carter, Phys. Rev. Lett. **47**, 1514 (1981).

[8] P. D. Cottle, J. W. Holcomb, T. D. Johnson, K. A. Stuckey, S. L. Tabor, P. C. Womble, S. G. Buccino, and F. E. Durham, Phys. Rev. C **42**, 1254 (1990).

[9] S. L. Tabor, P. D. Cottle, C. J. Gross, U. J. Hüttmeier, E. F. Moore, and W. Nazarewicz, Phys. Rev. C **39**, 1359 (1989).

[10] G. Winter, L. Funke, R. Schwengner, H. Prode, R. Wirowski, N. Nicholay, A. Dewald, and P. von Brentano, Z. Phys. A **343**, 369 (1992).

[11] G. D. Johns, J. Döring, J. W. Holcomb, T. D. Johnson, M. A. Riley, G. N. Sylvan, P. C. Womble, V. A. Wood, and S. L. Tabor, Phys. Rev. C **50**, 2786 (1994).

[12] J. W. Holcomb, T. D. Johnson, P. C. Womble, P. D. Cottle, S.

L. Tabor, F. E. Durham, and S. G. Buccino, Phys. Rev. C **43**, 470 (1991).
[13] J. Döring, R. Schwengner, L. Funke, H. Rotter, G. Winter, B. Cederwall, F. Linden, A. Johnson, A. Atac, J. Nyberg, and G. Sletten, Phys. Rev. C **50**, 1845 (1994).
[14] J. Döring, L. Funke, R. Schwengner, and G. Winter, in *Nuclear Structure in the Nineties*, edited by N. Johnson (Oak Ridge, TN, 1990), p. 84.
[15] J. Döring, L. Funke, R. Schwengner, and G. Winter, Phys. Rev. C **48**, 2524 (1993).
[16] L. Lühmann, M. Debray, K. P. Lieb, W. Nazarewicz, B. Wörmann, J. Eberth, and T. Heck, Phys. Rev. C **31**, 828 (1985).
[17] T. D. Johnson, T. Glasmacher, J. W. Holcomb, P. C. Womble, S. L. Tabor, and W. Nazarewicz, Phys. Rev. C **46**, 516 (1992).
[18] J. Heese, N. Martin, C. J. Gross, W. Fieber, K. P. Lieb, A. Kuhnert, K. H. Maier, and X. Sun, Phys. Rev. C **41**, 1553 (1990).
[19] G. N. Sylvan, J. E. Purcell, J. Döring, J. W. Holcomb, G. D. Johns, T. D. Johnson, M. A. Riley, P. C. Womble, V. A. Wood, and S. L. Tabor, Phys. Rev. C **48**, 2252 (1993).
[20] E. Roeckl, D. Lode, and W. Pessara, Z. Phys. **266**, 123 (1974).
[21] G. Winter, J. Döring, W. D. Fromm, L. Funke, P. Kemnitz, H. Prade, and E. Will, Nucl. Phys. **A367**, 95 (1981).
[22] A. J. Kreiner, M. A. J. Mariscotti, C. Baktash, E. der Mateosian, and P. Thieberger, Phys. Rev. C **24**, 148 (1981).
[23] N. Martin, C. J. Gross, J. Heese, and K. P. Lieb, J. Phys. G **15**, L123 (1989).
[24] M. A. Deleplanque, C. Gerschel, N. Perrin, and B. Ader, J. Phys. (France) **35**, L237 (1974).
[25] S. L. Tabor, M. A. Riley, J. Döring, P. D. Cottle, R. Books, T. Glasmacher, J. W. Holcomb, J. Hutchins, G. D. Johns, T. D. Johnson, T. Petters, O. Tekyi-Mensah, P. C. Womble, L. Wright, and J. X. Saladin, Nucl. Instrum. Methods Phys. Res. B **79**, 821 (1993).
[26] D. C. Radford, Nucl. Instrum. Methods Phys. Res. A **361**, 297 (1995).
[27] S. L. Tabor, Phys. Rev. C **45**, 242 (1992).
[28] W. Nazarewicz, J. Dudek, R. Bengtsson, T. Bengtsson, and I. Ragnarsson, Nucl. Phys. **A435**, 397 (1985).
[29] U. J. Hüttmeier, C. J. Gross, D. M. Headly, E. F. Moore, S. L. Tabor, T. M. Cormier, P. M. Swertka, and W. Nazarewicz, Phys. Rev. C **37**, 118 (1988).
[30] H. Schäfer, A. Dewald, A. Gelberg, U. Kaup, K. O. Zell, and P. von Brentano, Z. Phys. A **293**, 85 (1979).
[31] S. E. Larsson, G. Leander, and I. Ragnarsson, Nucl. Phys. **A307**, 189 (1978).
[32] Paul B. Semmes and Ingemar Ragnarsson, in *High Spin Physics and Gamma Soft Nuclei*, edited by J. X. Saladin, R. A. Sorensen, and C. M. Vincent (World Scientific, Singapore, 1990), p. 500.
[33] T. Bengtsson and I. Ragnarsson, Nucl. Phys. **A436**, 14 (1985).
[34] J. W. Holcomb, J. Döring, T. Glasmacher, G. D. Johns, T. D. Johnson, M. A. Riley, P. C. Womble, and S. L. Tabor, Phys. Rev. C **48**, 1020 (1993).
[35] G. D. Johns, J. Döring, R. A. Kaye, G. N. Sylvan, and S. L. Tabor, Phys. Rev. C **55**, 660 (1997).